Research Article

Alexander von Finck*, Steffen Wilbrandt, Olaf Stenzel and Sven Schröder

Reducing light scattering from surface contaminations by thin film design

DOI 10.1515/aot-2017-0027
Received April 10, 2017; accepted April 23, 2017; previously published online June 12, 2017

Abstract: In most applications, contamination of optical thin film coatings is inevitable over time. State-of-the art approaches to tackle this problem are usually based on two strategies – avoiding contamination or removing already existing contamination. We demonstrate that the coating design can be tailored to reduce light scattering and stray light arising from particle contamination. This allows reducing the optical symptoms (light scattering) rather than trying to address the inevitable cause of the problem (contamination) itself. This new approach can consequently be easily combined with state-of-the-art approaches.

Keywords: invisibility cloaks; multilayer design; particles; protective coatings; scattering; scattering particles.

OCIS codes: 230.3205; 310.4165; 350.4990; 310.1515; 290.0290; 290.5850.

1 Introduction

Contaminations located on even a single surface of optical components are capable of tremendously reducing the performance of the entire optical system. Typical contaminations relevant for optical applications are usually particles (dust) but also fluids from the environment or remnants from human interaction. These contaminations contribute additional scattered light, which in turn leads to (i) increased straylight, (ii) reduced throughput (reduced transmissions or reflectance), and (iii) a broadened point spread function of the optical system [1].

***Corresponding author: Alexander von Finck,** Fraunhofer Institute for Applied Optics and Precision Engineering, Albert-Einstein-Strasse 7, 07745 Jena, Germany, e-mail: alexander.finck@iof.fraunhofer.de
Steffen Wilbrandt, Olaf Stenzel and Sven Schröder: Fraunhofer Institute for Applied Optics and Precision Engineering, Albert-Einstein-Strasse 7, 07745 Jena, Germany

State-of-the art approaches to tackle this problem can be subdivided into two basic strategies – avoiding contamination or removing existing contamination:

- Contamination can be avoided, or at least the probability of contamination can be reduced, e.g. by utilizing electrostatic fields that act as a dust repellent, by capping layers that are chemically inert to contamination, or simply by encapsulating the optical system where possible.
- Removing (or at least a reduction) of already existing contamination is usually performed by manual cleaning procedures. Other techniques involve self-cleaning (superhydrophobic) micro- or nanostructures ('lotus effect') [2, 3], or photoactive top layers that disintegrate particles when exposed to UV irradiation [4].

However, in most cases, contamination is inevitable over time and may require either cleaning or even a substitution of the affected components. Still, cleaning of optics usually worsens the performance compared to the clean and newly fabricated component; cleaning also poses a risk as improper cleaning is much worse than no cleaning [5]. Cleaning or substitutions are even not always an option, e.g. for space applications or integrated optics.

We propose a thin film coating design technique that allows reducing the optical symptoms (contamination-induced light scattering) rather than trying to address the inevitable cause of the problem (contamination itself) [6]. This new approach can be easily combined with state-of-the-art approaches. Moreover, the technique can be used to reduce light scattering from defects or to reduce light scattering from nanostructures that are necessary for, e.g. superhydrophobic surfaces [7, 8].

In the following sections, the fundamental approach is described, and achievable parameters are discussed based on simulations. A proof-of-principle demonstrator is designed and fabricated containing two different coating designs with different sensitivity to contamination. The manufactured coatings are, then, artificially contaminated with particles. Experiments are conducted to quantify contamination-related light scattering losses.

2 Theoretical background

Light scattering distributions are quantified by the angle-resolved scattering (ARS) function defined as the power ΔP_s of the light that is scattered into the solid angle $\Delta\Omega_s$, normalized to that solid angle and to the incident light power P_i [1, 9, 10]:

$$\mathrm{ARS}(\theta_s, \varphi_s) = \frac{\Delta P_s(\theta_s, \varphi_s)}{P_i \Delta\Omega_s}, \tag{1}$$

where φ_s and θ_s are the azimuthal and polar scattering angles (see Figure 1), respectively. For normal incidence, integration of the ARS in the hemisphere within $\theta_s = 2°$ and $\theta_s = 85°$ allows calculating the total scattering (TS) according to ISO13696 [11]. For different integration limits, the quantity integrated scattering (S) is used. From ARS measurements that were performed in the plane of incidence, TS can be calculated for isotropic scattering samples. ARS is identical to the bidirectional scattering distribution function (BSDF) scaled by a factor of $\cos\theta_s$ [10], yet, ARS corresponds to the normalized intensity, while BSDF corresponds to the normalized luminance.

Theories, based on first-order perturbation models, were developed to connect the ARS to roughness descriptive surface properties. These theories were experimentally verified to be very accurate [1, 12–14], but are limited to smooth surfaces with $\sigma \ll \lambda$ (which, in fact, holds for the vast majority of optical coatings). In contrast to single surface scattering, predicting light scattering from multilayer coatings is more complex as interference effects have to be considered [15–17]. The ARS of a thin film stack of N layers is given by Ref. [16]:

$$\mathrm{ARS}(\varphi_s, \theta_s) = \sum_{i=0}^{N}\sum_{j=0}^{N} F_i F_j^* \mathrm{PSD}_{ij}(f_x, f_y), \tag{2}$$

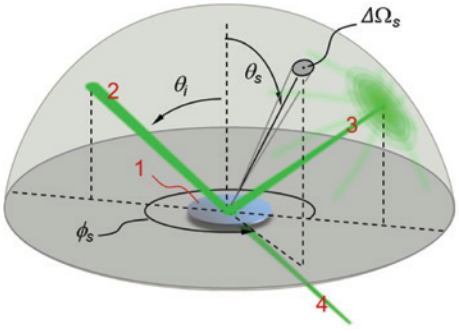

Figure 1: Light scattering geometry and definitions: 1 – sample, 2 – incident beam, 3 – reflected beam, 4 – transmitted beam, θ_i – angle of incidence, θ_s – polar scattering angle, φ_s – azimuth scattering angle.

where F_i denotes the optical factor at the i-th interface and F_j^* the conjugate complex optical factor at the j-th interface. The optical factors are closely related to the field-strength distribution inside multilayer coating and contain information about polarization states, scattering geometries, and dielectric constants. The power spectral density functions PSD_{ij} represent the i-th interface's PSD function (for $i=j$) and its cross correlation properties (for $i \neq j$). The PSD is determined from a surface profile by means of a Fourier transform [1] and, consequently, contains both vertical and lateral roughness information; its integration over a certain spatial frequency range results in the (bandwidth limited) rms roughness σ [13]. The spatial frequencies (f_x, f_y) and the scattering angles are connected by the grating equation [1].

Light scattering of particles on top of optical surfaces can be accurately predicted utilizing the Bobbert-Vlieger (BV) model [18, 19]. The model is based on the Mie theory and allows calculating the light scattering distribution of spherical particles on top of substrates. An extension of the model enables predicting particle light scattering on top of multilayer coatings [20]. The model holds for sphere diameters in the order of the wavelength of the incident light and for multiple particles that are separated far enough (such that an interaction between the spheres can be neglected). The fundamental derivation of the model is based on the electromagnetic fields interacting with the sphere, including the incident wave, the reflected incident wave by the substrate, as well as the reflection of the field scattered by the sphere, itself (multiple scattering).

3 Approach

In order to reduce the absorption of single layers of a multilayer stack, the field strength inside the volume of the corresponding layer has to be reduced by tailoring the coating design [21, 22]. Light scattering of thin film coatings is closely related to the field-strength distribution inside the multilayer stack [23], and hence, a similar approach could be fruitful. However, the physical mechanism of light scattering is fundamentally different to absorption: While absorption occurs inside the material volume, light scattering arises from the boundaries of different refractive indices/materials. Hence, in order to optimize light scattering by a tailored thin film design, a different strategy has to be pursued: To reduce light scattering, for example, from a single layer of a multilayer stack, the field strength at the layer interface(s) has to be reduced. To reduce light scattering from particles, moreover, interference effects and

interaction with the mirrored image of the particle itself (as described in the previous section) have to be considered.

Yet, modifying the standing electric field strength at the position of a particle, e.g. by adapting the protection layer thickness of a simple protected aluminum mirror [Al/Al_2O_3] effectively allows tailoring its light scattering characteristic. Figure 2 (left) shows the calculated TS caused by surface contaminations as a function of the Al_2O_3 layer thickness for illumination wavelengths of 405 nm, 532 nm, and 640 nm. The data was obtained utilizing the BV model [24] for particles with a diameter of 200 nm and for normal incidence. Compared to an unprotected aluminum coating (which corresponds to an Al_2O_3 layer thickness of 0 nm in Figure 2), the simulations predict a possible reduction of contamination-induced scattering by a factor of 35 at $\lambda = 640$ nm in the first minimum of the layer thickness. At lower wavelengths, or rather at larger particle diameter/wavelength relations, a reduction of contamination scattering is also feasible but grows less effective with factors of 19 (for $\lambda = 532$ nm) and 2.4 (for $\lambda = 405$ nm), respectively.

Varying the thickness of the Al_2O_3 layer, of course, also changes the specular performance of the design. The specular reflectance is plotted in Figure 2 (right) as a function of the Al_2O_3 layer thickness; the minima are slightly out of phase for 532 nm and 640 nm compared to the TS of the particles. This effect can be related to field-strength distribution effects inside this coating layout [25]. On the one hand, particle scattering correlates well with the average field inside the contamination zone, although this neglects interference effects and multiple scattering. Yet, a small offset in the optimum layer thickness can be observed (see Figure 3, left). On the other hand, the specular reflectance is minimized where the field strength at the Al_2O_3/air interface reaches a maximum (see Figure 3, right). This, in turn, leads to a minimized field above the surface inside a contamination zone of $\lambda/2$ thickness, which in this example coincidentally approximates the 200 nm particle diameter. A more complex design or other particle/wavelength relations, however, give more degrees of freedom to achieve a maximized reflectance with minimized contamination-induced light scattering.

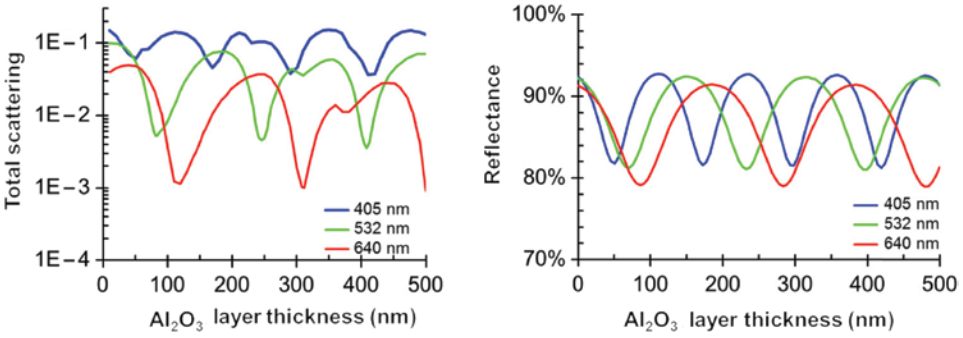

Figure 2: Left: simulated TS according to the BV model of 200 nm particles at illumination wavelengths of $\lambda = 405$ nm, 532 nm, and 640 nm. Right: specular reflectance of the coating design.

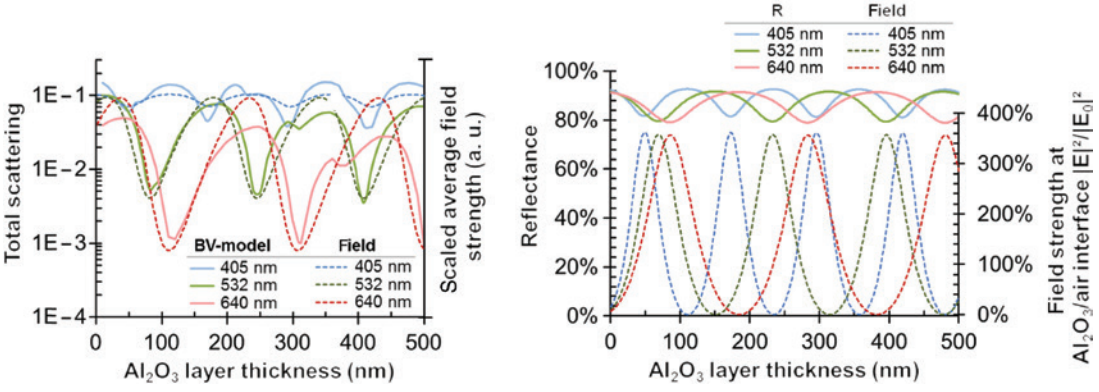

Figure 3: Left: simulated TS as in Figure 2 (solid lines) compared to the average field strength inside the contamination zone above the surface (dashed lines). For a better comparability, the field strength is plotted with a different offset for each wavelength and on a linear scale. Right: specular reflectance of the coating design compared to the field strength at the Al_2O_3/air interface.

In order to design a coating with minimized contamination scattering, the simulations show that the field above the surface in the contamination zone can be used as a compliant parameter for optical thin film design software. Fine tuning the design should be subsequently performed by light scattering calculations.

4 Sample preparation and experimental setup

In order to demonstrate the sensitivity of coating design to contamination-induced light scattering, two different Al/Al_2O_3 thin film coatings are investigated under equal conditions. For this purpose, the two designs were deposited by evaporation [26] on a single polished BK7 substrate (50 mm diameter): one coating design on each sample half (see Figure 4). Only design 2 was optimized for reduced particle scattering for a given set of parameters (illumination wavelength of $\lambda = 640$ nm, angle of incidence 60°, and particles with a diameter of 200 nm) by adapting the Al_2O_3 layer thickness to 144 nm. This results in a minimized field strength in the contamination zone just above the surface (Figure 4, right).

Both coating designs exhibit a similar specular reflectance at the optimized illumination wavelength of 640 nm with 95% and 88% for designs 1 and 2, respectively. However, the spectral reflectance of design 2 features pronounced minima at 300 nm and 840 nm illumination wavelengths where the Al_2O_3 coating fulfills the phase condition for anti-reflection.

The sample was then contaminated with polystyrene particles (200 nm diameter), which allows neglecting absorption effects for the experiments in the visible spectrum. In order to contaminate both sample halves equally, the particles were dissolved in distilled water, and each fluid droplet was run over both coatings 1 and 2. For a quantitative analysis of the contamination degree, atomic force microscopy (AFM) measurements (field size 10×10 µm²) were performed on both coatings in the contaminated area using a Dimension Icon from Bruker (Santa Barbara, CA, USA). Agglomerations were observable in the topographic scans; however, in the non-agglomerated areas, 0.027 particles per µm² were found on coating 1, while on coating 2, a similar contamination degree of 0.025 particles per µm² was derived. Hence, a similar degree of contamination was achieved for both coatings.

For the light scattering analysis presented in the next section, the multi-wavelength scatterometer ALBATROSS-TT was utilized. The instrument was developed at Fraunhofer IOF in Jena and can be used for hemispherical measurements of the ARS, BSDF, reflectance, and transmittance at different parameters (polarization, wavelength, etc.). A more detailed description of the instrument can be found in Refs. [27, 28]. Especially helpful was the capability to perform measurements at the identical position for different illumination wavelengths. This was crucial because this allows excluding systematical errors caused by even smallest deviations in the measurement position on these potentially lateral inhomogeneous samples between wavelength changes.

The spectral photometry measurements in the next section have been performed using a Lambda 950 scanning spectrophotometer from Perkin Elmer (Waltham, MA, USA) equipped with the General Purpose Optical Bench (GPOB). For absolute measurement of the reflectance at 6° angle of incidence, a VN accessory developed at Fraunhofer IOF has been used [29, 30].

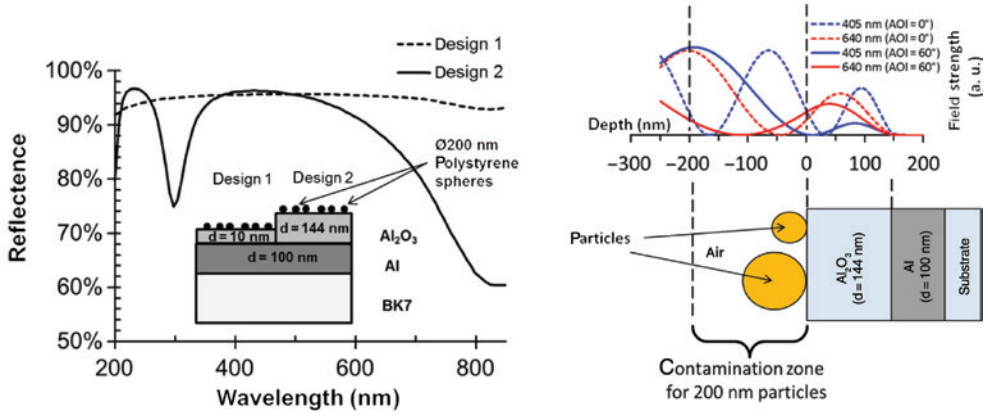

Figure 4: Left: two different reflective coatings were deposited on a single demonstrator sample and artificially contaminated. Right: field distributions of design 2 optimized for an illumination wavelength of $\lambda = 640$ nm, particles with a diameter of 200 nm, and 60° angle of incidence (AOI).

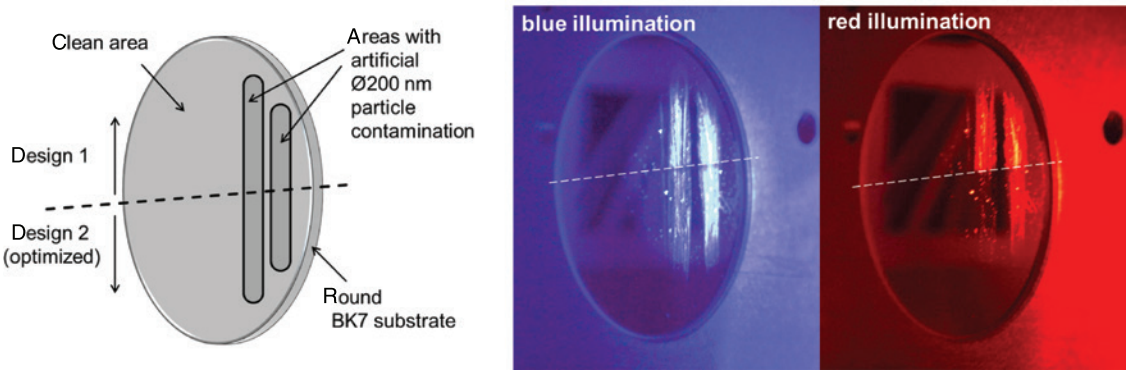

Figure 5: Left: schematic of the locally contaminated sample. Right: photographs of the sample at different illumination wavelengths.

5 Light scattering and reflectance analysis

Figure 5 shows a sketch as well as photographs of the prepared sample under different illuminations. Already with the naked eye, the contamination is visible on both coating halves under blue illumination. Also, agglomerations can be recognized by the structured inhomogeneous texture. However, the average degree of contamination in the contaminated areas looks identical for both coating designs, in agreement with the AFM analysis. For red illumination, however, the contaminated areas on coating 2 are almost not noticeable compared to coating 1. Only light scattering at isolated positions can be observed where the particles pile up to build agglomeration structures larger than the optimized contamination zone.

For a quantitative analysis, ARS measurements were performed at 405 nm and 640 nm illumination wavelengths at an incident angle of 60°. Measurement positions inside the clean area as well as in the contaminated area were chosen. At the clean positions (Figure 6), both coatings demonstrate the typical wavelength scaling ($\sim 1/\lambda^4$) that can be observed for light scattering from the topography of smooth single surfaces. The light scattering level exhibits a similar level for both coatings.

At positions in the contaminated area, however, both coatings exhibit a completely different behavior. For coating 1, a clearly reduced wavelength scaling is observable, and at 405 nm illumination, both coatings exhibit a similar light scattering level. These observations are rather not surprising and would be expected for samples with the same contamination degree and where contamination scattering dominates surface scattering.

However, at $\lambda = 640$ nm, the light scattering level of coating 2 is about one order of magnitude lower than the ARS at $\lambda = 405$ nm and the ARS of design 1. The TS of design 2 was found to be reduced by a factor of 6.4 compared to design 1; the ARS was reduced up to a factor of about 14.

Simulations utilizing the BV model are plotted in dotted lines based on the contamination degrees derived by the topography measurements. They show a good agreement to the measurements; however, it can be observed that (i) the simulations underestimate the overall light scattering level and that (ii) wavelength scaling for design 1 is less pronounced in the measurements. This can be explained by agglomeration scattering effects that are not covered by the simulation and which were not included in the topography analysis to derive the contamination degree. That is, the effective contamination degree was actually higher than derived by AFM; the model does not include multiple scattering events between different particles, and the simulations were not performed for particles with different distances to the sample surface and outside the contamination zone.

The effect of light scattering losses caused by contamination on the spectral reflectance was further analyzed by spectral photometry measurements. The measurements were performed at clean and contaminated positions on both coatings (Figure 7), respectivley. Because of technical reasons, the measurements were performed at 6° incident angle instead of 60°. It can be observed that the specular reflectance of both coatings is considerably reduced by contamination scattering. This allows calculating the spectrally resolved contamination-induced integrated scattering $S \equiv \Delta R$ by the difference in the specular reflectance of the clean (R_{clean}) and contaminated ($R_{\text{contaminated}}$) coatings, respectively (see Figure 8, left). The integration limits of S are given by the geometry of the utilized spectrophotometer and do not necessarily correspond to TS.

Contamination-induced scattering was found to be about six times lower for the optimized design 2 – possibly

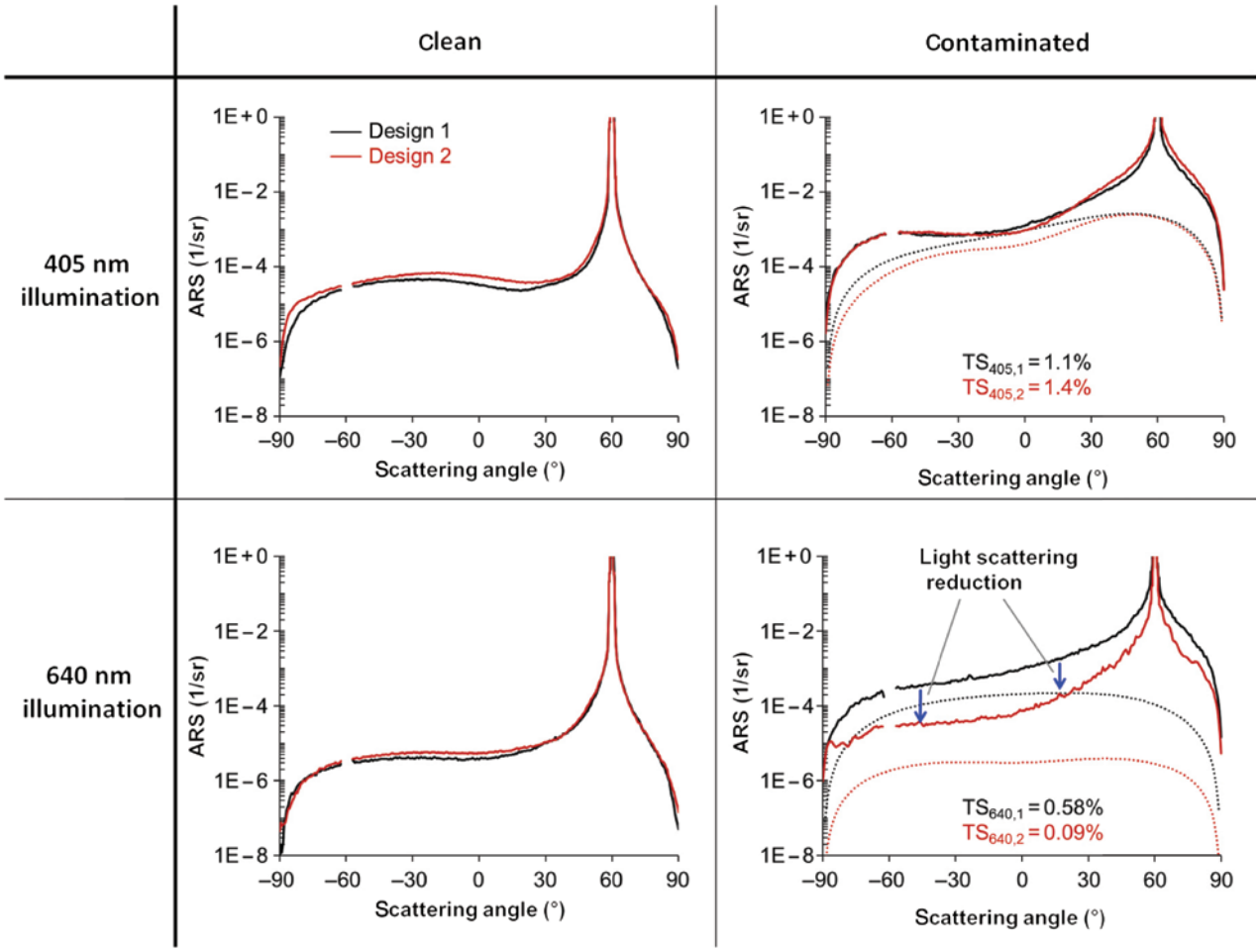

Figure 6: ARS measurements (solid lines) of both coating designs at 405 nm and 640 nm. The measurements were performed in the clean as well as the contaminated areas. Contamination scattering was also simulated using the BV model (dotted lines).

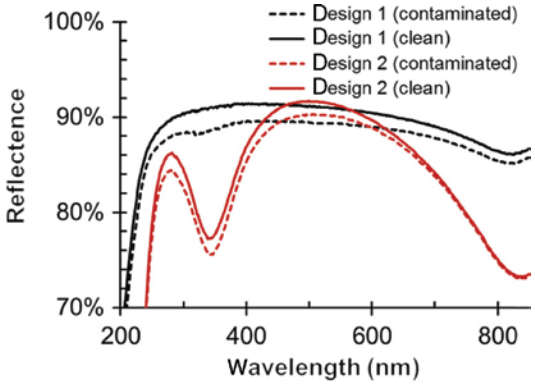

Figure 7: Measured specular reflectance by spectral photometry (6° incident angle) of the clean and contaminated coatings.

by a factor of 10 at IR wavelengths where the results are limited by the spectral photometry measurement uncertainty. Spectrally resolved light scattering simulations were performed for normal incidence (Figure 8, right). The general shape shows a good correlation to the measurements; however, the light scattering was again underestimated by the simulations for the same reasons already discussed above (particle agglomerations).

6 Summary

In order to reduce light scattering arising from surface contaminations, a new approach was proposed. In contrast to state-of-the-art techniques to tackle this problem, the optical symptoms of contamination (light scattering) are reduced rather than trying to prevent contamination itself. By simulations, it could be shown that the total scattering at $\lambda = 640$ nm from ø200 nm particles on a thin film coating can be reduced by a factor of 35 by tailoring the coating design. It could be further shown that the field strength in the contamination zone above the surface correlates with surface contamination scattering, although

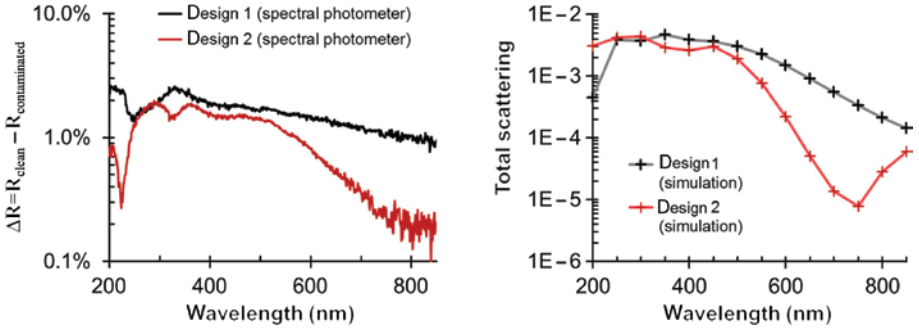

Figure 8: Left: decrease in the reflected power caused by contamination as determined by spectral photometry for both coatings. Right: simulated TS by contamination for both coatings.

with a small offset in the optimum layer thickness. This is especially helpful, as the field strength is a more adequate input for common optical thin film design software tools and can, thus, be used as a design criterion to tailor coatings for minimized contamination scattering. However, fine tuning the design should be subsequently performed by light scattering calculations. A demonstrator sample was fabricated with a different coating design on each sample half. Both sample halves were locally equally contaminated. Light scattering and spectral photometry measurements on clean and contaminated positions were performed, demonstrating a reduction of the contamination-induced light scattering by a factor of about 6. Deviations to the simulations were traced to agglomeration scattering.

Acknowledgments: The authors gracefully acknowledge Angela Duparré (IOF) for her support and the fruitful discussions. We also want to thank Yuan Wang, Tobias Herffurth, Nadja Felde, and Luisa Coriand (all IOF) for very helpful discussions and experimental support.

References

[1] J. C. Stover, 'Optical Scattering: Measurement and Analysis, 3rd ed. (SPIE Press, Bellingham, WA, 2012).
[2] M. Flemming, L. Coriand and A. Duparré, J. Adhes. Sci. Technol. 23, 381–400 (2009).
[3] N. Felde, L. Coriand, A. Duparré and A. Tünnermann, J. Coat. Sci. Technol. 3, 100–108 (2016).
[4] A. Linsebigler, G. Lu and J. Yates Jr, Chem. Rev. 95, 735–758 (1995).
[5] J. M. Bennett and L. Mattsson, Introduction to Surface Roughness and Scattering, 2nd ed. (Optical Society of America, Washington, DC, 1999).
[6] A. von Finck, S. Schröder, O. Stenzel, S. Wilbrandt, A. Duparré, et al., 'Optische Beschichtung und Verfahren zur Herstellung einer optischen Beschichtung mit verminderter Lichtstreuung', Patent pending (2015).
[7] A. Duparré and L. Coriand, in 'Advances in Contact Angle, Wettability and Adhesion', Ed. By K. L. Mittal (Scrivener Publishing LLC, Beverly, MA, 2013) pp. 193–202.
[8] L. Coriand, M. Mitterhuber, A. Duparré and A. Tünnermann, Appl. Opt. 50, C257–C263 (2011).
[9] A. Duparré, in 'Encyclopedia of Modern Optics', Ed. By R. D. Guenther, D. G. Steel and L. Bayvel (Elsevier, Amsterdam, 2004), pp. 314–321.
[10] S. Schröder, A. von Finck and A. Duparré, Adv. Opt. Technol. 4, 361–375 (2015).
[11] 'Optics and optical instruments—test methods for radiation scattered by optical components', ISO 13696:2002, 2002.
[12] R. D. Jacobson, S. R. Wilson, G. A. Al-Jumaily, J. R. McNeil, J. M. Bennett, et al., Appl. Opt. 31, 1426–1435 (1992).
[13] A. Duparré, J. Ferre-Borrull, S. Gliech, G. Notni, J. Steinert, et al., Appl. Opt. 41, 154–171 (2002).
[14] C. Deumie, R. Richier, P. Dumas and C. Amra, Appl. Opt. 35, 5583–5594 (1996).
[15] P. Bousquet, F. Flory and P. Roche, J. Opt. Soc. Am. 71, 1115–1123 (1981).
[16] A. Duparré and S. Kassam, Appl. Opt. 32, 5475–5480 (1993).
[17] C. Amra, J. Opt. Soc. Am. A 11, 197–210 (1994).
[18] P. Bobbert and J. Vlieger, Phys. A Stat. Mech. Appl. 137, 209–242 (1986).
[19] J. Kim, S. Ehrman, G. Mulholland and T. Germer, Appl. Opt. 43, 585–591 (2004).
[20] J. H. Kim, S. H. Ehrman, G. W. Mulholland and T. A. Germer, Appl. Opt. 41, 5405 (2002).
[21] J. Trenkler, H.-J. Mann and U. Nothelfer, 'Reflektives Optisches Element und EUV-Lithographiegerät,' Patent WO 002,004,079,753 (2003).
[22] H. A. Macleod, Thin-Film Optical Filters, 4th ed. (CRC Press, Boca Raton, FL, USA, 2010), pp. 584–591.
[23] S. Schröder, D. Unglaub, M. Trost, X. Cheng, J. Zhang, et al., Appl. Opt. 53, A35–A41 (2014).
[24] Light scattering simulations were performed using the software MIST: T. A. Germer, 'Modeled Integrated Scatter Tool (MIST)', available from http://physics.nist.gov/scatmech.
[25] Field strength and reflectance were calculated using the Software OptiLayer: A. V. Tikhonravov and M. K. Trubetskov. 'OptiLayer thin film software', http://www.optilayer.com (2003).
[26] S. Wilbrandt, O. Stenzel, H. Nakamura, D. Wulff-Molder, A. Duparré, et al., Appl. Opt. 53, A125–A130 (2014).

[27] A. von Finck, M. Trost, S. Schröder and A. Duparré, Opt. Express 23, 33493–33505 (2015).
[28] A. von Finck, T. Herffurth, S. Schröder, A. Duparré and S. Sinzinger, Appl. Opt. 53, A259–A269 (2014).
[29] O. Stenzel, S. Wilbrandt, K. Friedrich and N. Kaiser, Vakuum Forschung Praxis 21, 15–23 (2009).
[30] O. Stenzel, Optical Coatings. Material Aspects in Theory and Practice (Springer-Verlag Berlin Heidelberg, 2014).